論文 / 著書情報
Article / Book Information

Title	Dense Multipath Component Characteristics in 11 GHz Band Indoor Environments
Authors	Kentaro Saito, Jun-ichi Takada, Minseok Kim
Citation	IEEE Transactions on Antennas and Propagation, vol. 65, no. 9, pp. 4780-4789
Pub. date	2017, 9
Copyright	(c) 2017 IEEE. Personal use of this material is permitted. Permission from IEEE must be obtained for all other uses, in any current or future media, including reprinting/republishing this material for advertising or promotional purposes, creating new collective works, for resale or redistribution to servers or lists, or reuse of any copyrighted component of this work in other works.
DOI	http://dx.doi.org/10.1109/TAP.2017.2728087
Note	This file is author's final version.

Dense Multipath Component Characteristics in 11GHz-band Indoor Environments

Kentaro Saito, *Member, IEEE,* Jun-ichi Takada, *Senior Member, IEEE,* and Minseok Kim, *Member, IEEE,*

***Abstract*—In the next-generation mobile communication system, the higher frequency bands from C band to V band are expected to be utilized because it has the potential to improve network capacity drastically by the available wideband spectrum. Since the characteristics of reflected and scattered radio waves from surrounding environments in those bands are thought to be quite different than at lower frequencies, the clarification of its influence on the Multiple-Input Multiple-Output (MIMO) transmission performance is a critical issue. In this paper, we focused on the characteristics of diffuse scattering in X band, and conducted the MIMO channel measurements in indoor environments in the 11 GHz band. The frequency, angular, and polarization domain Dense Multipath Component (DMC) propagation parameters were jointly estimated by using the RiMAX-based estimator. The measurement result showed the existence of significant DMC, which is thought to have originated from the floor, the ceiling as well as the walls. The angular spreads of the DMC tended to increase, and their decay factor tended to decrease as the room size decreased. It is also shown that the existence of DMC significantly affected the eigenvalue structure of the MIMO channel, which defines the MIMO transmission performance. The result is expected to be utilized for novel MIMO channel modelling in X band that includes the DMC contribution.**

***Index Terms*—diffuse scattering, Dense Multipath Component, MIMO channel modeling**

I. Introduction

USER traffic in the mobile network is increasing drastically owing to the spread of tablet computers and various application services. Recently, the next-generation mobile communication systems such as the fifth generation (5G) system [1] [2] have been widely investigated in order to accommodate the increasing user traffic. In the 5G system, the utilization of higher frequency bands from C band to V band for the mobile communication has become a hot research topic because it has the potential to improve the network capacity drastically by using the available wideband spectrums. Furthermore, massive Multiple-Input Multiple-Output (MIMO) technologies are expected to be employed in those frequency bands for achieving higher order beamforming and spatial multiplexing data transmission.

The higher frequency bands have not been used for the mobile communication. Especially in indoor environments, it is thought that radio waves will be scattered from various objects in the environment. Diffuse scattering is thought to consist mainly of the irregular scattering from rough surfaces of objects [3]. Although it might be expected that diffuse scattering arising from rough surfaces would be more prominent in X band compared to the Ultra High Frequency (UHF) band due to X-band's shorter wavelength, additional attenuation may also reduce the effect. It is known that diffuse scattering affects the MIMO transmission performance significantly in some communication scenarios [4] [5] [6]. However, the contribution of diffuse scattering is not considered in de facto standard channel models such as the 3GPP Spatial Channel Model (SCM) [7], ITU-R M.2135 channel model [8], and WINNER II channel model [9]. Therefore, the clarification of the influence of diffuse scattering on MIMO channel characteristics is a critical issue for the higher-frequency-band MIMO channel modeling.

In previous works on diffuse scattering, scattering characteristics from a rough wall of a building were measured and the modeling method was introduced to include those contributions into ray tracing simulations [10] [11]. Although the Power Delay Profile (PDP), angular spread, and polarization characteristics of diffuse scattering were also evaluated through ray trace simulations [12] [13] [14], the evaluation correctness relies on the accuracy of assumed environment map used in the simulations.

In previous works on the MIMO channel modelling, the contributions of diffuse scattering were directly estimated and parametrized from MIMO channel measurements by the RiMAX algorithm [15] [16] [17]. In the RiMAX algorithm, coherent waves such as direct waves and regular reflection waves are modeled deterministically as Specular Multipath Component (SMC), and the composition of vast amounts of incoherent plane waves due to diffuse scattering is modeled stochastically as Dense Multipath Component (DMC). The DMC is characterized by autocorrelations of the signal component, and only the frequency domain correlation has been discussed in the RiMAX algorithm [15] [16] [17]. In [18], the DMC frequency domain parameters were estimated from measurement data of a Line-of-Sight (LoS) industrial environment in the 3 GHz band. The result showed that the power ratio of the DMC to the total received power ranged from 23 % to 38 %, and the PDP of the DMC almost followed the exponential decay distribution that is described in the RiMAX algorithm. The polarization domain characteristics of the DMC were also investigated in an industrial hall in the 1.3 GHz band [19], in a large hall in the 1.3 GHz band [20], and in urban environments in the 4.5 GHz band [21]. The results showed that the DMC had polarization dependencies. The angular-domain characteristics of the DMC were investigated in indoor environments in the 5.3 GHz band [22]. The results showed that the angular power profile of the DMC correlated

Kentaro Saito and Jun-ichi Takada are with the School of Environment and Society, Tokyo Institute of Technology, Tokyo, Japan (e-mail:saitouken@ide.titech.ac.jp).

Minseok Kim is with Department of Electrical and Electronic Engineering, Niigata University, Niigata, Japan.

to it of the SMC, as also described in [23]. To deal with angular and polarization characteristics of the DMC quantitatively, the extensions of the RiMAX algorithm have been proposed. In [24] [25], the von Mises distribution [26] was used for representing the angular profile of the DMC. The angular-domain autocorrelation of the DMC is calculated by convolution of the DMC angular profile and the array response. In [27], the extension of the DMC polarization domain parameters and the parameter estimation method was proposed.

In the past literature, the discussion on DMC characteristics is limited to lower frequency bands below 6GHz. Furthermore, the investigation only focused on frequency domain DMC parameters, without a quantitative analysis on angular domain parameters in actual environments. The contribution of our work is the clarification of DMC characteristics in X band through 11 GHz band MIMO channel measurements [28]. We have extended the conventional RiMAX algorithm for the joint estimation of the DMC propagation parameters in the frequency, angular, and polarization domains to evaluate the characteristics of the DMC in a quantitative way [29] [30]. This paper expands our previous work in [29] [30] by providing a more comprehensive investigation on the DMC characteristics in three different indoor environments, particularly in the following aspects. We evaluated the propagation parameter distributions of the DMC in each indoor environment, and discussed the influences of the environments on the DMC characteristics. We also clarified to what extent the DMC contributes to the eigenvalues structure of the MIMO channel by comparing the measurement data and the data reconstructed from the estimated propagation parameters. Finally, we investigated the originating source of the DMC by utilizing the 3-dimensional (3D) virtual array method.

The rest of this paper is structured as follows. The received signal model and the DMC propagation parameter estimation method are described in Section II. Then the MIMO channel measurement setup in the 11 GHz band in indoor environments is presented in Section III. The measurement results and the DMC propagation parameters characteristics are presented in Section IV. Finally, the conclusion and avenues for future work are described in Section V.

II. RiMAX-based DMC Propagation Parameter Estimation

A. Signal Model and Parameter Estimation Method

In Fig. 1, the assumed signal model of the MIMO propagation channel [27] [30] is shown. The signal consists of the sum of SMC and DMC. The SMC is modeled by the superposition of plane waves that are deterministically defined by propagation parameters. The SMC propagation parameter vector of the i-th path $\boldsymbol{\theta}_{\mathrm{s},i}$ consists of the propagation delay $\tau_{\mathrm{s},i}$, the azimuth Angle of Arrival (AAoA) $\phi_{\mathrm{R},i}$, the co-elevation Angle of Arrival (EAoA) $\theta_{\mathrm{R},i}$, the azimuth Angle of Departure (AAoD) $\phi_{\mathrm{T},i}$, the co-elevation Angle of Departure (EAoD) $\theta_{\mathrm{T},i}$, and the complex amplitude vector $\boldsymbol{\gamma}_i = [\gamma_{\mathrm{s,vv},i}, \gamma_{\mathrm{s,vh},i}, \gamma_{\mathrm{s,hv},i}, \gamma_{\mathrm{s,hh},i}]$. In the signal model, the SMC of the i-th path $\boldsymbol{s}(\boldsymbol{\theta}_{\mathrm{s},i}) \in \mathbb{C}^{N_{\mathrm{F}}N_{\mathrm{R}}N_{\mathrm{T}}\times 1}$ is defined as follows. Here, N_{F} is the number of subcarriers , N_{R} is the number of Receiver (Rx) antennas, and N_{T} is the number of Transmitter (Tx) antennas.

$$\boldsymbol{\theta}_{\mathrm{s},i}=[\tau_{\mathrm{s},i}, \phi_{\mathrm{R},i}, \theta_{\mathrm{R},i}, \phi_{\mathrm{T},i}, \theta_{\mathrm{T},i}, \boldsymbol{\gamma}_i] \quad (1)$$

$$\boldsymbol{s}(\boldsymbol{\theta}_{\mathrm{s},i})=\boldsymbol{\alpha}_{\mathrm{F}}(\tau_{\mathrm{s},i}) \otimes \boldsymbol{\alpha}_{\mathrm{R}}(\phi_{\mathrm{R},i}, \theta_{\mathrm{R},i}) \otimes \boldsymbol{\alpha}_{\mathrm{T}}(\phi_{\mathrm{T},i}, \theta_{\mathrm{T},i})\boldsymbol{\gamma}_i \quad (2)$$

Here, $\boldsymbol{\alpha}_{\mathrm{F}}(\tau_{\mathrm{s},i})$ is the frequency transfer function of the impulse function $\delta(\tau - \tau_{\mathrm{s},i})$, and $\boldsymbol{\alpha}_{\mathrm{R}}$ and $\boldsymbol{\alpha}_{\mathrm{T}}$ are the Rx and the Tx array antenna responses, respectively. $\otimes$ represents the Kronecker product.

The DMC is modeled by the signal component, which is stochastically determined by the delay-domain DMC propagation parameter $\boldsymbol{\theta}_{\mathrm{d,F}}$ and the angular-polarization domain DMC propagation parameter $\boldsymbol{\theta}_{\mathrm{d,A}}$ as follows:

$$\boldsymbol{\theta}_{\mathrm{d,F}}=[\alpha_0, \alpha_1, \beta_{\mathrm{d}}, \tau_{\mathrm{d}}] \quad (3)$$

$$\boldsymbol{\theta}_{\mathrm{d,A}}=[\mu_{\mathrm{R}}, \mu_{\mathrm{T}}, \kappa_{\mathrm{R}}, \kappa_{\mathrm{T}}, \gamma_{\mathrm{d,vv}}, \gamma_{\mathrm{d,vh}}, \gamma_{\mathrm{d,hv}}, \gamma_{\mathrm{d,hh}}, \gamma_{\alpha}] \quad (4)$$

In [15] [16], the PDP of the DMC is modeled as the following exponential decay distribution by using the delay-domain DMC parameters.

$$f_{\mathrm{F}}(\tau) = \begin{cases} \alpha_0 & (\tau < \tau_{\mathrm{d}}) \\ \alpha_1/2 & (\tau = \tau_{\mathrm{d}}) \\ \alpha_1 e^{-B_{\mathrm{d}}(\tau-\tau_{\mathrm{d}})} & (\tau > \tau_{\mathrm{d}}) \end{cases} \quad (5)$$

In [23] [24] [25], the angular power spectrum of the DMC is modeled by the von Mises distribution [26]. In the literature, the Rx-side angular power spectrum is defined as follows.

$$f_{\mathrm{R}}(\phi) = \frac{1}{2\pi \mathrm{I}_0(\kappa_{\mathrm{R}})} e^{\kappa_{\mathrm{R}}\cos(\phi-\mu_{\mathrm{R}})} \quad (6)$$

Here, $\mathrm{I}_0(\cdot)$ is the modified Bessel function of the first kind and the order is zero, μ_{R} is the center AAoA of the DMC, and κ_{R} is a parameter which represents the angular spread of the von Mises distribution. The angular spread decreases and the distribution approaches to the normal distribution as κ_{R} increases. The angular spread σ_{R} is approximated by $\sigma_{\mathrm{R}} = \kappa_{\mathrm{R}}^{-0.5}$ in the case of large κ_{R}.

The frequency domain correlation matrix $\boldsymbol{R}_{\mathrm{F}}(\boldsymbol{\theta}_{\mathrm{d,F}}) \in \mathbb{C}^{N_{\mathrm{F}}\times N_{\mathrm{F}}}$ and the angular-polarization domain correlation matrix $\boldsymbol{R}_{\mathrm{A}}(\boldsymbol{\theta}_{\mathrm{d,A}}) \in \mathbb{C}^{N_{\mathrm{R}}N_{\mathrm{T}}\times N_{\mathrm{R}}N_{\mathrm{T}}}$ are calculated from the power density distribution defined in eq. (5) and (6). Finally, the DMC correlation matrix $\boldsymbol{R}(\boldsymbol{\theta}_{\mathrm{d,F}}, \boldsymbol{\theta}_{\mathrm{d,A}})$ is calculated as follows:

$$\boldsymbol{R}(\boldsymbol{\theta}_{\mathrm{d,F}},\boldsymbol{\theta}_{\mathrm{d,A}}) = \boldsymbol{R}_{\mathrm{F}}(\boldsymbol{\theta}_{\mathrm{d,F}}) \otimes \boldsymbol{R}_{\mathrm{A}}(\boldsymbol{\theta}_{\mathrm{d,A}}) \quad (7)$$

The estimation procedure is explained as follows. First, the SMC parameter $\boldsymbol{\theta}_{\mathrm{s},i}$ is estimated from the measured data $\boldsymbol{x}$ by the SAGE algorithm [31]. Next, the delay, angular and polarization domain propagation parameters of the DMC are next estimated by the RiMAX-based algorithm. The detailed procedure is explained in [30].

B. Stochastic MIMO Channel Generation Method

In this section, the MIMO channel generation method based on the estimated propagation parameters is explained. Because the contribution of the radio propagation channel and the array antenna characteristics to the MIMO channel are separately

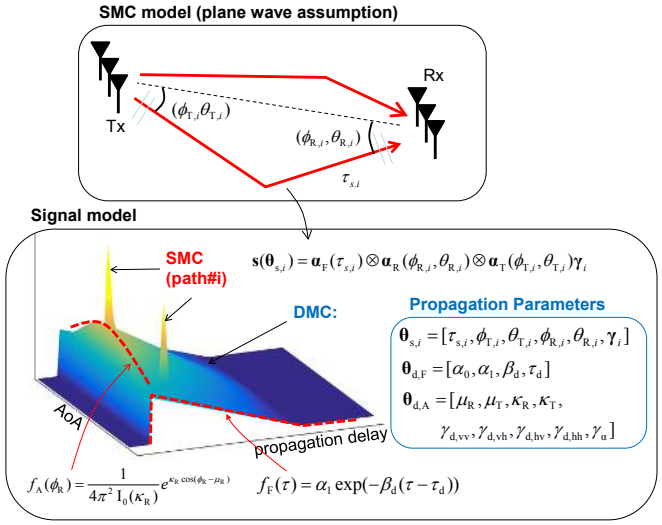

Fig. 1. The SMC and the DMC model of MIMO propagation channel.

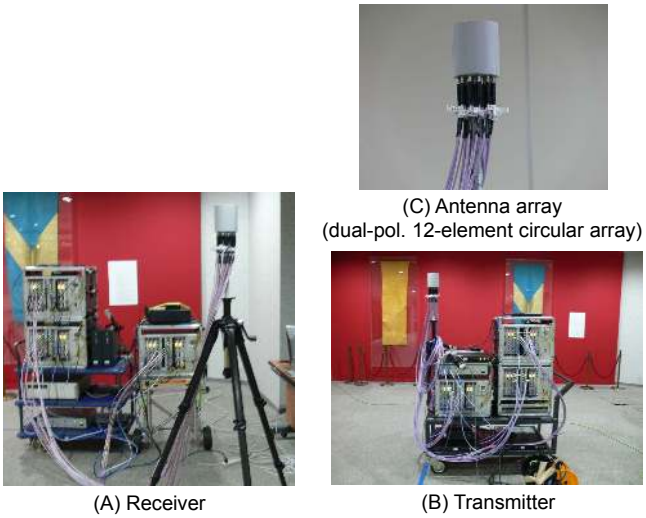

Fig. 2. Photos of 11-GHz-band channel sounder: ((A) Receiver, (B) Transmitter , and (C) Antenna Array).

modeled in the Geometry-based channel model explained in II-A, the MIMO channel reconstruction from the estimated propagation parameters is necessary to validate how accurately the MIMO channel characteristics are modeled. Generally, it is possible to synthesize MIMO channels even if we assume array antennas other than the one used in the measurement. The MIMO channel is synthesized from the propagation parameters $\boldsymbol{\theta}_{\mathrm{s},i}$, $\boldsymbol{\theta}_{\mathrm{d,F}}$, and $\boldsymbol{\theta}_{\mathrm{d,A}}$ and the array antenna responses $\boldsymbol{\alpha}'_{\mathrm{R}}$ and $\boldsymbol{\alpha}'_{\mathrm{T}}$ which are assumed for the channel generation.

In [15] [16], the generated MIMO channel $\boldsymbol{x}' \in \mathbb{C}^{N_{\mathrm{F}} N_{\mathrm{R}} N_{\mathrm{T}} \times 1}$ consists of the SMC of the i-th path $\boldsymbol{s}'(\boldsymbol{\theta}_{\mathrm{s},i})$ and the DMC $\boldsymbol{d}'(\boldsymbol{\theta}_{\mathrm{d,F}}, \boldsymbol{\theta}_{\mathrm{d,A}})$.

$$\boldsymbol{x}' = \sum_{i=1}^{I} \boldsymbol{s}'(\boldsymbol{\theta}_{\mathrm{s},i}) + \boldsymbol{d}'(\boldsymbol{\theta}_{\mathrm{d,F}}, \boldsymbol{\theta}_{\mathrm{d,A}}) \tag{8}$$

Here, $\boldsymbol{s}'(\boldsymbol{\theta}_{\mathrm{s},i})$ is deterministically generated from the SMC propagation parameters according to eq. (2). Because the DMC is modeled stochastically, $\boldsymbol{d}'(\boldsymbol{\theta}_{\mathrm{d,F}}, \boldsymbol{\theta}_{\mathrm{d,A}})$ is stochastically generated from the i.i.d. channel matrix $\boldsymbol{G} \in \mathbb{C}^{N_{\mathrm{F}} N_{\mathrm{R}} N_{\mathrm{T}} \times 1}$ and the correlation matrix $\boldsymbol{R}'(\boldsymbol{\theta}_{\mathrm{d,F}}, \boldsymbol{\theta}_{\mathrm{d,A}})$.

$$\boldsymbol{d}'(\boldsymbol{\theta}_{\mathrm{d,F}}, \boldsymbol{\theta}_{\mathrm{d,A}}) = \boldsymbol{L}\boldsymbol{G} \tag{9}$$

Here, $\boldsymbol{L}$ is the matrix that satisfies $\boldsymbol{L}\boldsymbol{L}^{\mathrm{H}} = \boldsymbol{R}'(\boldsymbol{\theta}_{\mathrm{d,F}}, \boldsymbol{\theta}_{\mathrm{d,A}})$.

III. 11 GHz-band Indoor MIMO Channel Measurement

We conducted MIMO channel measurements in the 11 GHz band in several indoor environments to clarify the frequency, angular and polarization characteristics of the DMC in X band. The specifications of the 11-GHz-band MIMO channel sounder that we have developed [32] is shown in Table I. Photos of Tx, Rx, and the antenna array are also shown in Fig. 2. The Tx/Rx antenna arrays were 12-element circular arrays with dual-polarized patch antennas. Therefore, 24-by-24 MIMO channel matrices with 400 MHz bandwidth were obtained in the measurement. The Tx/Rx antenna heights were set to 1.7 m.

TABLE I
Measurement Parameters.

Channel sounder parameters	
Center frequency	11 GHz
Bandwidth	400 MHz
Transmit power (per antenna)	10 mW
Transmit signal	Multitone signal
Number of Tone	2048
Tx/Rx antenna array	12-element circular array (12 V-pol. and 12 H-pol.)
Tx antenna height	1.7 m
Rx antenna height	1.7 m (moving measurement) 1.7 m, 1.714 m, 1.728 m, 1.742 m (3D measurement)
Data analysis parameters	
Maximum path number	10, 20, 40, 80, or 120
Maximum iteration number (both SAGE and RiMAX)	20
Path discarding threshold ξ	20 dB

The measurements were conducted in 3 indoor environments: a room, a hall, and a museum. The floor layouts and photos of each environment are shown in Fig. 3, and 4. In the room and in the hall, there was no furniture except for a few chairs and tables. In the museum, there were several tables, chairs and interior structures such as pillars. The sizes of those areas were about 18 m $\times$10 m $\times$3 m, 30 m $\times$10 m $\times$3 m, and 30 m $\times$20 m $\times$6.5 m, respectively. We conducted two kinds of measurements. The first kind of measurement is a moving measurement, where the Rx was set at fixed points in the areas, and then the Tx was moved along the measurement courses at a constant speed of approximately 0.25 m/s. The channels were measured at every 1.4 sec. during the measurements. The Rx points and measurement courses are shown in Fig. 3. The numbers of the Rx points were 2 in the room and in the museum, and 3 in the hall. The number of the courses were

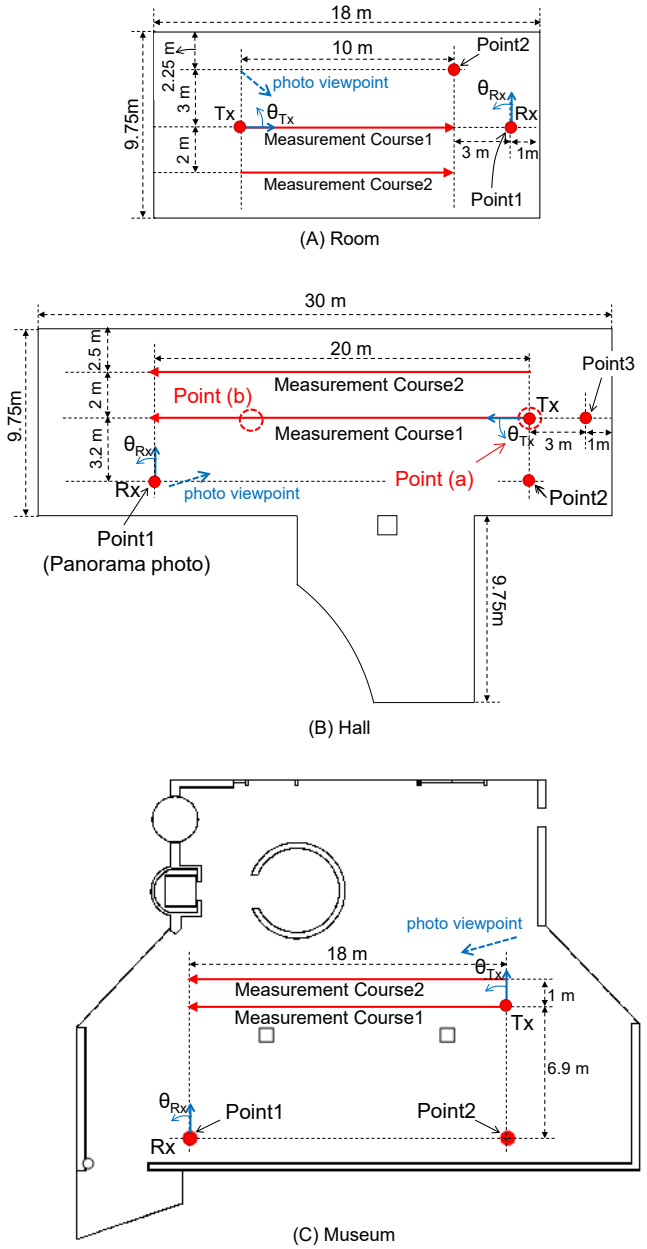

Fig. 3. The floor layouts of measurement areas: ((A) Room, (B) Hall, and (C) Museum)).

2 in all areas. The Tx/Rx array directions are also shown, and the AAoA and the AAoD were defined from the front directions of the instruments in a counter-clockwise direction. The statistical distributions of the propagation parameters in each environment were estimated from the measurements. The second kind of measurement is a 3D measurement by using the virtual array method. In this measurement, the Rx was fixed at Point 1 and the Tx was fixed at Point (a) in the hall. To investigate the elevation domain propagation characteristics, we conducted the measurements by changing the Rx antenna height from 1.7 m, 1.714 m, 1.728 m, to 1.742 m. The step length of the height approximately corresponded to the half wave length, which is 13.6 mm in the 11 GHz band. We evaluated the SMC and Residual Signal Component (RSC) characteristics by assuming four measurement data as a 96-by-24 MIMO channel matrix.

In the data analysis, the SMC parameters were first estimated by the SAGE algorithm [31]. Then the frequency, angular, and polarization domains DMC propagation parameters were estimated by the RiMAX-based estimator that was explained in Section II. In the data analysis, the maximum specular path numbers were changed from 10, 20, 40, 80, and 120. The path discarding threshold ξ was 20 dB. Paths whose powers were lower than the highest path power by ξ were discarded. The RSC, which is the residual signal component after subtracting the SMC from the measured data, was calculated from the estimation results. The signal ratio of the RSC to the whole measured data, and the delay-angular characteristics of the RSC were discussed. Next, the delay, angular, and polarization domain DMC propagation parameters were estimated. Although the DMC characteristics are defined by the correlation matrix $\boldsymbol{R}$ as shown in eq. (7), there is an ambiguity in terms of the normalization of $\boldsymbol{R}_{\mathrm{F}}(\boldsymbol{\theta}_{\mathrm{d,F}})$ and $\boldsymbol{R}_{\mathrm{A}}(\boldsymbol{\theta}_{\mathrm{d,A}})$. For example, $m\boldsymbol{R}_{\mathrm{F}}(\boldsymbol{\theta}_{\mathrm{d,F}}) \otimes \boldsymbol{R}_{\mathrm{A}}(\boldsymbol{\theta}_{\mathrm{d,A}}) = \boldsymbol{R}_{\mathrm{F}}(\boldsymbol{\theta}_{\mathrm{d,F}}) \otimes m\boldsymbol{R}_{\mathrm{A}}(\boldsymbol{\theta}_{\mathrm{d,A}})$. In this paper, we normalized the DMC power gain $\boldsymbol{\gamma_{\mathrm{d}}} = [\gamma_{\mathrm{d,vv}}, \gamma_{\mathrm{d,vh}}, \gamma_{\mathrm{d,hv}}, \gamma_{\mathrm{d,hh}}, \gamma_{\alpha}]$ for presenting the results.

$$\gamma_{\mathrm{d,vv}} + \gamma_{\mathrm{d,vh}} + \gamma_{\mathrm{d,hv}} + \gamma_{\mathrm{d,hh}} + \gamma_{\alpha} = 1 \tag{10}$$

The DMC propagation parameter distributions in each environment are then shown. Finally, 4-by-4 MIMO channel matrices were generated from the estimated propagation parameters, and the eigenvalue structures of the generated channels were compared with the measured data.

IV. 11 GHz-band Channel Measurement Result

A. Residual Signal Component Characteristics

Fig. 5 shows the residual power ratios of all cases of maximum path numbers. The residual power ratio p_{RSC} is defined by measured data $\boldsymbol{x}$ and RSC $\boldsymbol{r}$ as follows.

$$\boldsymbol{r} = \boldsymbol{x} - \sum_{i=1}^{I} \boldsymbol{s}(\boldsymbol{\theta}_{\mathrm{s},i}) \tag{11}$$

$$p_{\mathrm{RSC}} = \frac{|\boldsymbol{r}|^2}{|\boldsymbol{x}|^2} \tag{12}$$

The figure shows the mean of the residual power ratios of all moving measurement snapshots in each area. Although the residual power ratios monotonically decreased as the maximum path number is increased, the slopes of the graphs became gradually smaller. The residual power ratios remained more than 30% in all cases. The RSC is thought to consist of DMC mainly, and the result showed the difficulty in modeling the DMC accurately by the superposition of a finite number of plane waves. The residual power ratio was highest in the room, followed by the hall, and then the museum. The reason is thought to be that the scattering of waves by the walls, floor, and ceiling was more significant in the small rooms. In this paper, we set the maximum path number to 80 for the following detailed evaluations. The residual power ratios were 0.47, 0.35, and 0.31, respectively.

Fig. 4. Photos of measurement areas: ((A) Room, (B) Hall, and (C) Museum)).

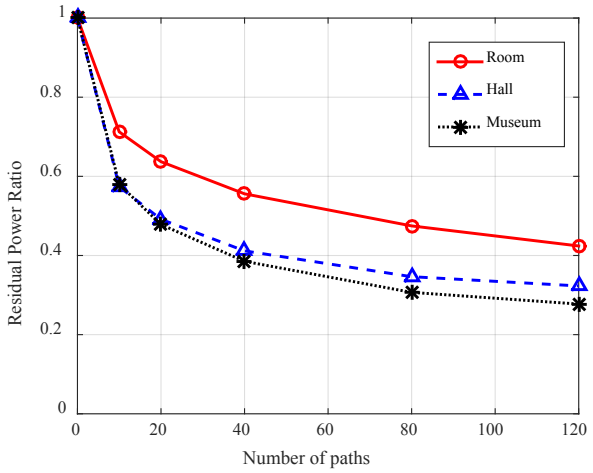

Fig. 5. Comparison of residual power ratio for various maximum path numbers in several environments

Next, we present the 3D measurement result. In Fig. 6, a panorama photo from the Rx-side view at Point 1 in the hall is shown. The delay-AAoA domain SMC estimation result of the 3D-measurement when the Tx was at Point (a) in Fig. 3 is also shown. In the SMC result, the paths formed some clusters. The first cluster was present approximately at 70 ns of the propagation delay and -80° of the AAoA. They are thought to be direct propagation paths from the Tx. There was also a cluster approximately at 120 ns of the propagation delay and 80° of the AAoA. It is thought to consist of the reflection paths from the left-side wall in the map. Other clusters that were reflected from the walls were also observed.

In Fig. 7, the PDP of the 3D measurement data, the SMC reconstructed from the SMC propagation parameters, and the RSC at Point (a) are shown. The result shows that although the part of the signal component whose propagation delay was approximately less than 200 ns was mainly estimated as the SMC, the other part remained as the RSC. The RSC remained significantly also in the early reflection region. The RSC PDP followed the exponential decay distribution, which is described in [15] [16]. The RSC peak level was approximately 10 dB lower than the SMC peak.

Fig. 8 shows the RSC power spectrum of both the delay-AAoA and delay-EAoA domains. As described in [22] [23], the RSC was distributed around the SMC that was shown in Fig. 6. Especially, the angular spread was wide in both azimuth and elevation domains in the early reflection region where the propagation delay was less than 200 ns. It indicates that the RSC consisted of the single bounce irregular scattering from the floor, ceiling, and walls in the region. In the multiple reflection region where the propagation delay was more than 200 ns, the RSC was mainly observed approximately at 80° and -80° of the AAoA and 90° of the EAoA. It shows that the RSC consisted of multiple reflection waves between the left-side wall and the right-side wall of the map. Because the RSC level was much higher in the early reflection region than the multiple reflection region, the DMC modeling in the early reflection region is thought to be important. The appropriate DMC modeling is also expected to improve the SMC estimation accuracy in the multiple reflection region because it is not detected correctly by the ML-based estimator due to the lower power compared with the peak power of the DMC.

B. DMC parameter distributions

In Fig. 9, the transitions of τ_{D}, μ_{R}, and μ_{T} when the Rx was fixed at point 1 and the Tx was moved along Course 1 in the hall are shown. τ_{D}, μ_{R}, and μ_{T} represent the peak position of the DMC in the delay and angular domains. In the figure, the LoS directions and the LoS propagation delays which are theoretically calculated are also shown. The result shows that the transitions of τ_{D}, μ_{R}, and μ_{T} were close to the values of LoS propagation. This result also shows that the scattering from the floor and the ceiling between the Tx and the Rx were one of the significant sources of diffuse scattering.

In Fig. 10, the Cumulative Distribution Functions (CDFs) of α_1 in all measurement areas are shown. α_1 represents the peak power of the DMC. To mitigate the influence of pathloss variations due to the distance differences between the Tx and the Rx, α_1 was normalized by the highest path gain of the paths, which almost corresponded to the LoS propagation path gain. The medians of α_1 ranged from -12 dB to -9 dB, and it was significantly higher than the value of -20 dB in an outdoor environment in the same frequency band [33]. The result showed that the contributions of the DMC to the MIMO channel characteristics are not negligible in X band.

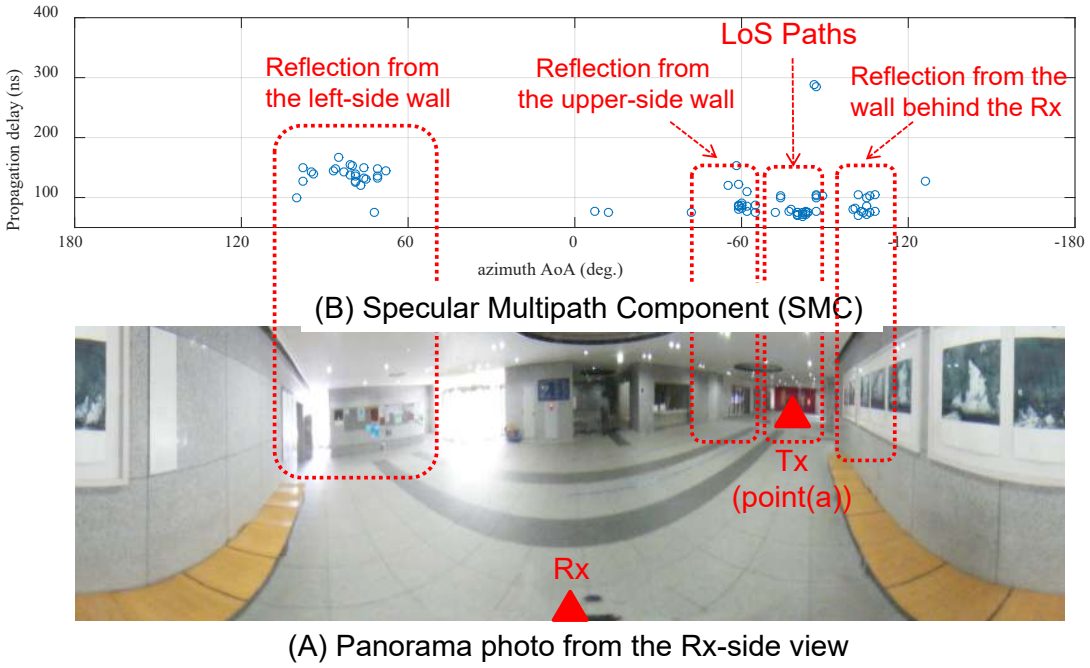

Fig. 6. 3D Measurement results at Point (a) in the hall ((A)Panorama photo from the Rx-side view, (B) Specular multipath component.

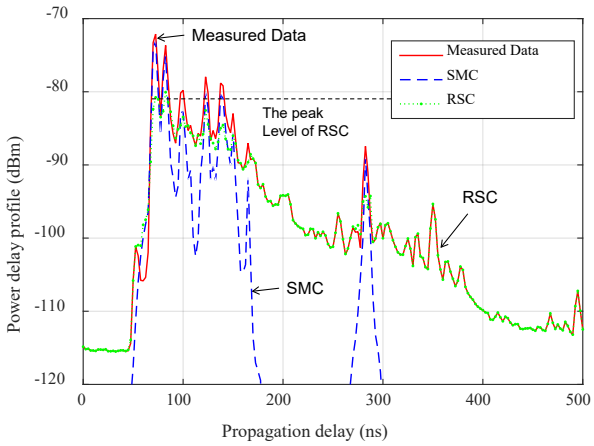

Fig. 7. The Power delay profile of 3D measurement at Point (a).

In Fig. 11, the CDFs of κ of both the Rx and the Tx side in all measurement areas are shown. κ represents the angular spread of the DMC. The medians of κ ranged from 0.4 to 0.8 in all the areas, and they corresponded to the range from 80° to 90° of the angular spreads. Although the DMC angular distribution was not uniform as described in [15] [16], the total spreads were quite large in indoor environments. Regarding α_1 and κ, the CDFs matched the normal distributions well. For practical purposes, we also showed the fitted lines of normal distributions in the figures. $n(\mu, \sigma)$ represents the normal distribution whose mean is μ and the standard deviation is σ.

In Table II, we summarized the estimated DMC propagation parameters. The means and the standard deviations of each parameter are presented. The Cross-Polarization Ratio (XPR) $\gamma_{\rm xpr}$, and the Co-Polarization Ratio (CPR) $\gamma_{\rm cpr}$ of the DMC were calculated from the DMC power gain $\boldsymbol{\gamma}_{\rm d}$ as follows:

$$\gamma_{\rm xpr} = \frac{\gamma_{\rm d,vv} + \gamma_\alpha}{\gamma_{\rm d,vh} + \gamma_\alpha} \tag{13}$$

$$\gamma_{\rm cpr} = \frac{\gamma_{\rm d,vv} + \gamma_\alpha}{\gamma_{\rm d,hh} + \gamma_\alpha} \tag{14}$$

We also showed the XPR and CPR of the SMC for the comparison. The XPR and CPR of the SMC were calculated by summing the path gains of each polarization setting $[|\gamma_{{\rm s,vv},i}|^2, |\gamma_{{\rm s,vh},i}|^2, |\gamma_{{\rm s,hv},i}|^2, |\gamma_{{\rm s,hh},i}|^2]$ for all the paths. The mean DMC XPRs ranged from 5.2 dB to 7.7 dB, which were 4 or 5 dB lower than the SMC XPRs. The DMC XPR tends to be several dBs lower than the SMC also in the lower frequency measurements [19] [20] [21]. The mean DMC CPRs were approximately 1 dB, which were almost the same as the SMC CPRs. The DMC had significant polarization dependencies. The reason why the DMC XPR was high is thought to be that the DMC mainly originated from diffuse scattering on the floor, the ceiling and walls in the area, and the polarization planes of the scattered waves were not changed significantly, because the scattered surfaces were almost horizontal or vertical.

$B_{\rm d}$ ranged from 18.2 MHz to 25.5 MHz, which were higher than the measurement results in the 3GHz band [18]. However, because the frequency characteristics also depend on the measurement environments, such as the floor layout and the wall materials, a careful comparison will be necessary. As shown in Fig. 5, the residual power ratios were highest in the room, followed by the hall, and then the museum. With respect to the differences of the DMC propagation parameters in each measurement area, the mean α_1 was highest in the room. In

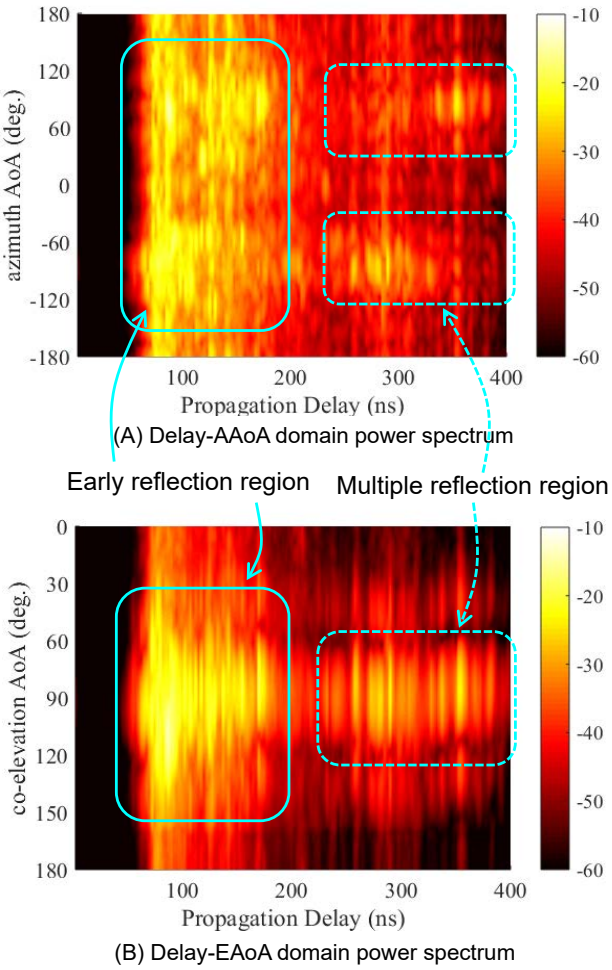

Fig. 8. The RSC power spectrum of 3D measurement ((a) Delay-AAoA domain, (b) Delay-EAoA domain).

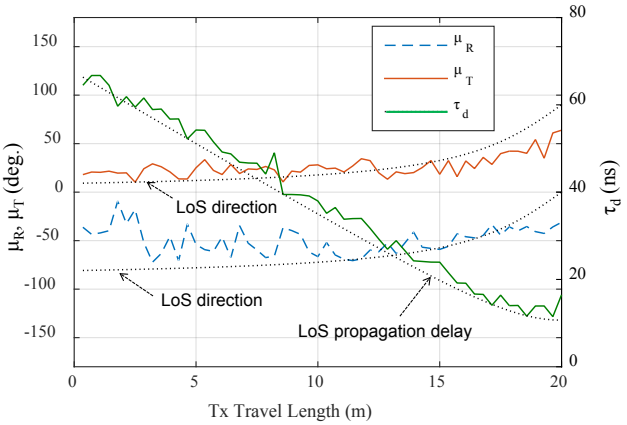

Fig. 9. The transitions of τ_{D}, μ_{R}, and μ_{T} in course 1 in the hall.

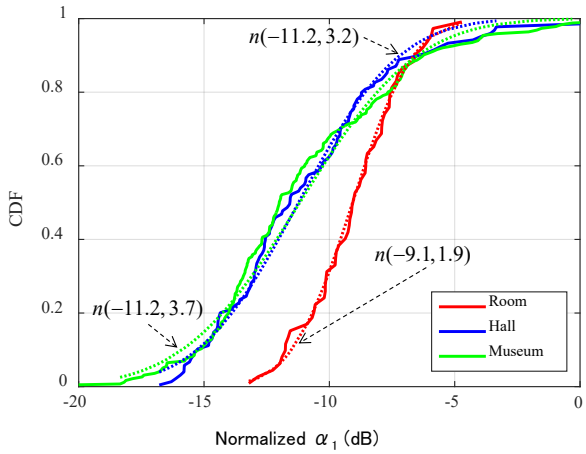

Fig. 10. α_1 CDF of each measurement area.

addition, the mean B_{d} and the mean κ were smallest in the room. These results showed that the influence of irregular scattering was more significant in the small room, which increased the DMC angular spread and decreased the DMC PDP decay factor. Those tendencies followed in the order of the hall and the museum. From the comparative results, it is thought that room size is one of the key factors that determine the characteristics of the DMC.

C. Channel Reconstruction and Eigenvalue Characteristics

The characteristics of MIMO channel matrices that were reconstructed from the propagation parameters are investigated for the validation of the estimation results. We assumed the same antenna responses as the measurement to clarify the influence of the DMC existence on the accuracy of the channel reconstruction. The matrices were reconstructed from the estimated SMC and DMC propagation parameters according to eq. (8) and eq. (9). Fig. 12 shows the received power of all MIMO channels when the Tx was at Point (b) and the Rx was at Point 1 in the hall. The received powers were calculated by summing the received powers of all delay bins. The figure shows the received power of the measured data, the data reconstructed only from the SMC, and the data reconstructed from both the SMC and the DMC. With respect to the radiated region of the co-polarized condition, the received powers were reconstructed fairly well by both methods. However, the received powers were significantly underestimated in the shadowing region in the case that the data were reconstructed only from the SMC. This is because the contribution of the DMC in the region was relatively higher than in the radiated region. The result shows that the received powers are not correctly reconstructed in the shadowing region without considering the DMC contribution.

Next, eigenvalues characteristics of the reconstructed MIMO channel matrices are investigated. The channel generation method is shown in Fig. 13. We selected 4-by-4 MIMO channel matrices from the whole channel data at each snapshot with a central focus on the LoS direction. In the spatially-separated MIMO (SS-MIMO) condition, only the vertical polarized propagation channels were selected. In the dual-polarized MIMO (DP-MIMO) condition, 2 vertically polarized propagation channels and 2 horizontally polarized

[1]The power is normalized by the highest path gain of the paths

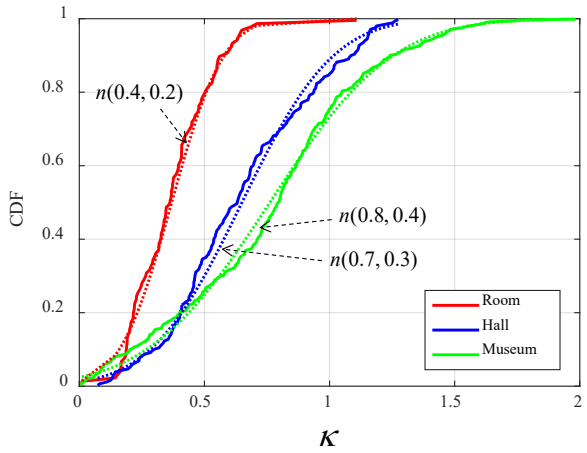

Fig. 11. κ CDF of each measurement area.

TABLE II
DMC PROPAGATION PARAMETERS SUMMARY.

DMC parameter	Room		Hall		Museum	
	mean	s.d.	mean	s.d.	mean	s.d.
$\alpha_1{}^1$ (dB)	-9.1	1.9	-11.2	3.2	-11.2	3.7
B_{d} (MHz)	18.2	1.8	21.8	3.2	25.5	3.6
$\kappa_{\mathrm{R,T}}$	0.4	0.2	0.7	0.3	0.8	0.4
XPR (dB)	7.7	0.6	6.8	0.7	5.2	0.8
CPR (dB)	1.5	0.3	1.0	0.9	1.1	1.5
SMC polarization characteristics (for references)						
XPR (dB)	11.4	1.6	10.1	1.3	10.7	1.4
CPR (dB)	1.1	1.4	1.0	1.9	1.4	1.7

propagation channels were selected. Fig. 14 and 15 show 4 eigenvalues CDFs of each MIMO condition. The figures show the mean eigenvalues of all subcarriers, and the eigenvalues are normalized by the medians of the first eigenvalues of the measured MIMO channels. In the SS-MIMO condition, the first eigenvalues were prominent owing to the strong LoS signal component, and they had good agreement with the measurement in both reconstruction methods. However, the second and the following eigenvalues were significantly underestimated in the case that the channel were reconstructed only from the SMC. The median eigenvalue reconstruction errors were -0.7 dB, -3.2 dB, -4.6 dB, and -7.8 dB, respectively. The errors were less than 1.4dB when the DMC contribution was considered, and this shows the validity of our DMC analysis results. In the DP-MIMO condition, although the first two prominent eigenvalues were fairly reconstructed in both reconstruction methods, the consideration of the DMC was also indispensable to improve the reconstruction accuracies of the following eigenvalues. The result showed that the DMC consideration is necessary to prevent the underestimation of the MIMO transmission performance.

V. CONCLUSION

In this paper, 11-GHz-band MIMO channel measurement results in LoS indoor environments was presented to clarify the propagation characteristics of the DMC in X band. We jointly estimated the frequency, angular and polarization domain DMC propagation parameters by the extended RiMAX based estimator to deal with the DMC contribution to the MIMO channel quantitatively. In the measurements, the residual power ratios when we assume only the SMC were almost more than 30% in all areas. Through the 3D measurement by using the virtual array method, we showed that the originating source of the RSC in the early reflection region is the irregular scattering from the floor, ceiling, and walls in the environment. The RSC was significant in the early reflection region, and its peak level was approximately 10 dB lower than the SMC peak. Although the frequency domain distributions of the DMC almost followed the RiMAX DMC model, the DMC had angular and polarization dependencies, which are not present in the RiMAX DMC model. The median DMC angular spreads were from 80° to 90°, and the DMC XPR was from 5.2 dB to 7.7 dB. The results also show that the angular spreads tended to increase and the decay factor tended to decrease as the room size decreased owing to more significant scattering effects from the environment.

For the validation of the modeling, the MIMO channel matrices were reconstructed from the estimated propagation parameters and compared with the measurement data. The comparative result showed that the receiving power was underestimated in the shadowing region if the DMC was not taken into account. The second and the following eigenvalues of the 4-by-4 MIMO channel matrices were also underestimated even in the radiated region. However, we found that the eigenvalues structure was reconstructed fairly well by considering the DMC contribution mainly focused on the RSC characteristics in the early reflection region, and the median reconstruction errors of eigenvalues were less than 2 dB.

Creating a novel higher frequency band MIMO channel model that includes the DMC contribution will be a future work.

ACKNOWLEDGMENT

This work was partly supported by "The research and development for expansion of radio spectrum resources" of The Ministry of Internal Affairs and Communications (MIC), JSPS KAKENHI Grant Number 15H04003, and JSPS KAKENHI Grant Number 16K18102.

REFERENCES

[1] T. S. Rappaport, S. Sun, R. Mayzus, H. Zhao, Y. Azar, K. Wang, G. N. Wong, J. K. Schulz, M. Samimi, and F. Gutierrez, "Millimeter Wave Mobile Communications for 5G Cellular: It Will Work!" *IEEE Access*, vol. 1, pp. 335–349, 2013.

[2] K. Sakaguchi, E. M. Mohamed, H. Kusano, M. Mizukami, S. Miyamoto, R. E. Rezagah, K. Takinami, K. Takahashi, N. Shirakata, H. Peng, T. Yamamoto, and S. Nanba, "Millimeter-Wave Wireless LAN and Its Extension toward 5G Heterogeneous Networks," *IEICE Transactions on Communications*, vol. 98, no. 10, pp. 1932–1948, 2015. [Online]. Available: http://ci.nii.ac.jp/naid/130005101277/

[3] P. Beckmann and A. Spizzichino, *The scattering of electromagnetic waves from rough surfaces*. Pergamon, New York, 1963.

[4] N. Czink, A. Richter, E. Bonek, J. P. Nuutinen, and J. Ylitalo, "Including Diffuse Multipath Parameters in MIMO Channel Models," in *Vehicular Technology Conference, 2007. VTC-2007 Fall. 2007 IEEE 66th*, Sept 2007, pp. 874–878.

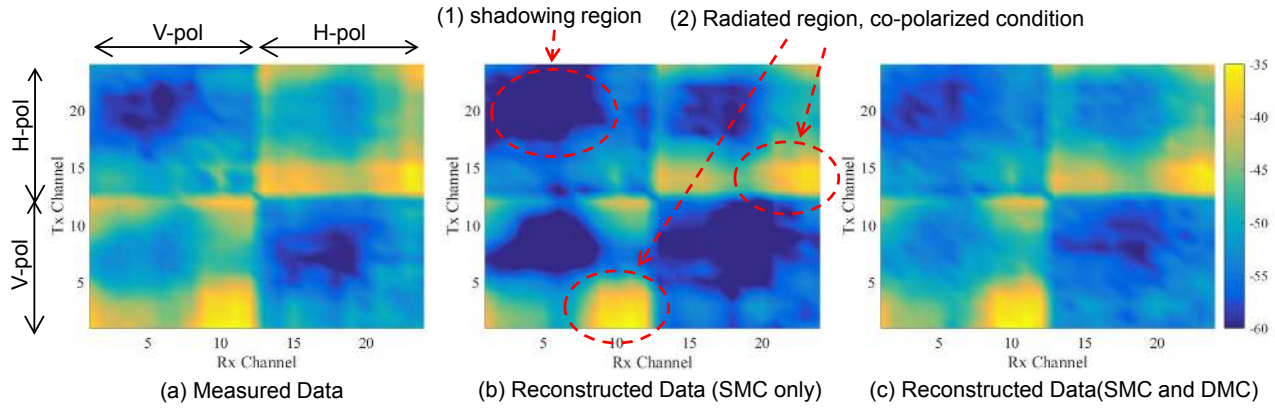

Fig. 12. The reconstructed MIMO channel at point(b) in the hall: ((a) measured data, (b) reconstructed data only from the SMC, and (c) reconstructed data from both the SMC and the DMC).

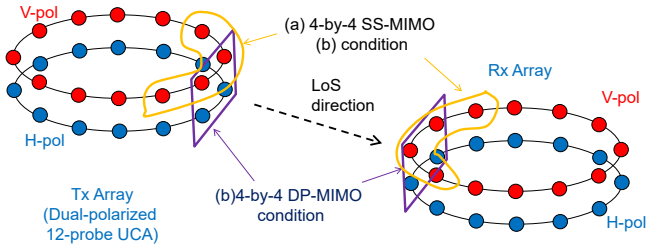

Fig. 13. Spatially-separated (SS) and dual-polarized (DP) 4-by-4 MIMO channel matrices generation method.

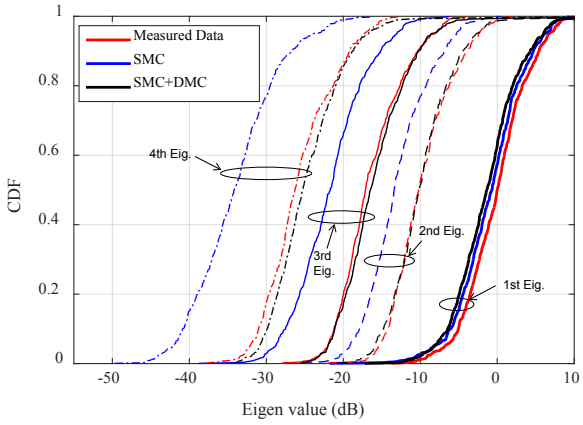

Fig. 14. Eigenvalues CDFs of SS-MIMO channel matrices.

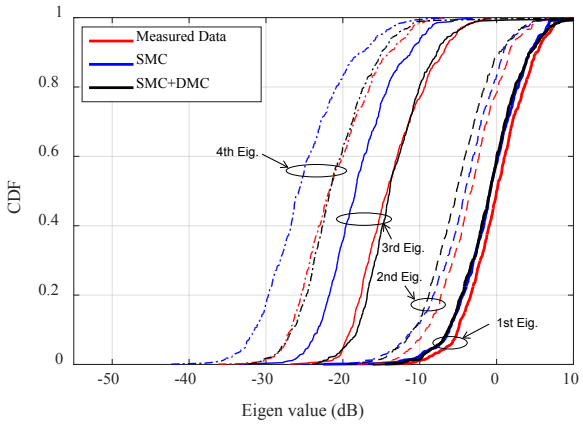

Fig. 15. Eigenvalues CDFs of DP-MIMO channel matrices.

[5] A. Richter, J. Salmi, and V. Koivunen, "Distributed scattering in radio channels and its contribution to MIMO channel capacity," in *Antennas and Propagation, 2006. EuCAP 2006. First European Conference on*, Nov 2006, pp. 1–7.

[6] A. Richter, "The Contribution of Distributed Scattering in Radio Channels to Channel Capacity: Estimation and Modeling," in *Signals, Systems and Computers, 2006. ACSSC '06. Fortieth Asilomar Conference on*, Oct 2006, pp. 951–955.

[7] 3GPP, *Spatial channel model for Multiple Input Multiple Output (MIMO) simulations (Release 7)* . 3GPP TR 25. 996, v7. 0. 0, 2007.

[8] ITU-R, *Guidelines for evaluation of radio interface technologies for IMT-Advanced* . Report ITU-R M.2135, 2009. [Online]. Available: http://www.itu.int/pub/R-REP-M.2135-2008/en

[9] P. Kyosti *et al.*, *WINNER II Channel Models* . IST-WINNER II D1.1.2, Nov 2007.

[10] V. Degli-Esposti, F. Fuschini, E. M. Vitucci, and G. Falciasecca, "Measurement and Modelling of Scattering From Buildings," *IEEE Transactions on Antennas and Propagation*, vol. 55, no. 1, pp. 143–153, Jan 2007.

[11] Y. Lostanlen and G. Gougeon, "Introduction of diffuse scattering to enhance ray-tracing methods for the analysis of deterministic indoor UWB radio channels (Invited Paper)," in *Electromagnetics in Advanced Applications, 2007. ICEAA 2007. International Conference on*, Sept 2007, pp. 903–906.

[12] E. M. Vitucci, F. Mani, V. Degli-Esposti, and C. Oestges, "A Study on Polarimetric Properties of Scattering from Building Walls," in *Vehicular Technology Conference Fall (VTC 2010-Fall), 2010 IEEE 72nd*, Sept 2010, pp. 1–5.

[13] F. Mani, F. Quitin, and C. Oestges, "Directional Spreads of Dense Multipath Components in Indoor Environments: Experimental Validation of a Ray-Tracing Approach," *IEEE Transactions on Antennas and Propagation*, vol. 60, no. 7, pp. 3389–3396, July 2012.

[14] E. M. Vitucci, F. Mani, V. Degli-Esposti, and C. Oestges, "Polarimetric Properties of Diffuse Scattering From Building Walls: Experimental Parameterization of a Ray-Tracing Model," *IEEE Transactions on Antennas and Propagation*, vol. 60, no. 6, pp. 2961–2969, June 2012.

[15] A. Richter, "Estimation of radio channel parameters: Models and algorithms ," Ph.D. dissertation, Technische Universitat Ilmenau, 2005.

[16] A. Richter and R. S. Thoma, "Joint maximum likelihood estimation of specular paths and distributed diffuse scattering," in *Vehicular Technology Conference, 2005. VTC 2005-Spring. 2005 IEEE 61st*, vol. 1, May 2005, pp. 11–15 Vol. 1.

[17] A. Richter, J. Salmi, and V. Koivunen, "An Algorithm for Estimation and Tracking of Distributed Diffuse Scattering in Mobile Radio Channels," in

Signal Processing Advances in Wireless Communications, 2006. SPAWC '06. IEEE 7th Workshop on, July 2006, pp. 1–5.
[18] E. Tanghe, D. P. Gaillot, M. Lienard, L. Martens, and W. Joseph, "Experimental Analysis of Dense Multipath Components in an Industrial Environment," *IEEE Transactions on Antennas and Propagation*, vol. 62, no. 7, pp. 3797–3805, July 2014.
[19] D. P. Gaillot, E. Tanghe, W. Joseph, P. Laly, V. C. Tran, M. Lienard, and L. Martens, "Polarization Properties of Specular and Dense Multipath Components in a Large Industrial Hall," *IEEE Transactions on Antennas and Propagation*, vol. 63, no. 7, pp. 3219–3228, July 2015.
[20] D. P. Gaillot, E. Tanghe, W. Joseph, P. Laly, B. Hanssens, M. Lienard, and L. Martens, "Polarization properties of specular and dense multipath components in a large industrial hall," in *General Assembly and Scientific Symposium (URSI GASS), 2014 XXXIth URSI*, Aug 2014, pp. 1–4.
[21] M. Landmann, K. Sivasondhivat, J. Takada, I. Ida, and R. Thoma, "Polarization Behavior of DiscreteMultipath and Diffuse Scattering in Urban Environments at 4.5 GHz ," *EURASIP Journal on Wireless Communications and Networking*, vol. 2007, 2007.
[22] J. Poutanen, J. Salmi, K. Haneda, V. M. Kolmonen, F. Tufvesson, and P. Vainikainen, "Propagation Characteristics of Dense Multipath Components," *IEEE Antennas and Wireless Propagation Letters*, vol. 9, pp. 791–794, 2010.
[23] J. Salmi, J. Poutanen, K. Haneda, A. Richter, V. M. Kolmonen, P. Vainikainen, and A. F. Molisch, "Incorporating diffuse scattering in geometry-based stochastic MIMO channel models," in *Antennas and Propagation (EuCAP), 2010 Proceedings of the Fourth European Conference on*, April 2010, pp. 1–5.
[24] C. B. Ribeiro, A. Richter, and V. Koivunen, "Stochastic Maximum Likelihood Estimation of Angle- and Delay-Domain Propagation Parameters," in *Personal, Indoor and Mobile Radio Communications, 2005. PIMRC 2005. IEEE 16th International Symposium on*, vol. 1, Sept 2005, pp. 624–628.
[25] C. B. Ribeiro, A. Richter, and V. Koivunen, "Joint Angular- and Delay-Domain MIMO Propagation Parameter Estimation Using Approximate ML Method," *IEEE Transactions on Signal Processing*, vol. 55, no. 10, pp. 4775–4790, Oct 2007.
[26] K.V.Mardia, *Statistics of Directional Data* . New York: Academic, 1972.
[27] M. Kaske and R. Thoma, "Maximum-likelihood based estimation of angular parameters of Dense-Multipath-Components," in *2015 9th European Conference on Antennas and Propagation (EuCAP)*, May 2015, pp. 1–6.
[28] M. Kim, Y. Konishi, Y. Chang, and J. Takada, "Large Scale Parameters and Double-Directional Characterization of Indoor Wideband Radio Multipath Channels at 11 GHz," *IEEE Transactions on Antennas and Propagation*, vol. 62, no. 1, pp. 430–441, Jan 2014.
[29] K. Saito, J. Takada, and M. Kim, "Characteristics Evaluation of Dense Multipath Component in 11GHz-band Indoor Environment," in *2016 10th European Conference on Antennas and Propagation (EuCAP)*, April 2016.
[30] K. Saito, J. Takada, and M. Kim, "Dense multipath component parameter estimation in 11GHz-band indoor environment," in *2016 IEEE 27th Annual International Symposium on Personal, Indoor, and Mobile Radio Communications (PIMRC)*, Sept 2016.
[31] J. A. Fessler and A. O. Hero, "Space-alternating generalized expectation-maximization algorithm," *IEEE Transactions on Signal Processing*, vol. 42, no. 10, pp. 2664–2677, Oct 1994.
[32] M. Kim, J. Takada, and Y. Konishi, "Novel Scalable MIMO Channel Sounding Technique and Measurement Accuracy Evaluation With Transceiver Impairments," *IEEE Transactions on Instrumentation and Measurement*, vol. 61, no. 12, pp. 3185–3197, Dec 2012.
[33] K. Saito, J. Takada, and M. Kim, "11 GHz Band MIMO Channel Characteristics in a Street Micro-Cell Environment," in *2017 11th European Conference on Antennas and Propagation (EuCAP)*, March 2017.

Kentaro Saito Kentaro Saito was born in Kanagawa, Japan, in 1977. He received his B.S. and Ph.D. degrees from the University of Tokyo, Japan, in 2002 and 2008, respectively. He joined NTT DOCOMO, Kanagawa, Japan, in 2002. Since then, he has been engaged in the research and development of mobile communication systems, and radio propagation. He joined Tokyo Institute of Technology, Japan in 2015. Since then, he has been engaged in research on radio propagation for mobile communication systems. Dr. Saito is a member of IEICE and IEEE.

Jun-ichi Takada (S89-M93-SM11) received the B.E., M.E., and D.E. degrees in electrical and electronic engineering from Tokyo Institute of Technology, Tokyo, Japan, in 1987, 1989, and 1992, respectively. From 1992 to 1994, he was a Research Associate with Chiba University, Chiba, Japan. From 1994 to 2006, he was an Associate Professor with Tokyo Institute of Technology, where he has been a Professor since 2006. From 2003 to 2007, he was also a Researcher with the National Institute of Information and Communications Technology, Kyoto, Japan. From 2007 to 2010, he was a Co-Chair of the Special Interest Group on Body Communications within EU COST Action 2100. His research interests include radio-wave propagation and channel modeling for mobile and short range wireless systems, regulatory issues of spectrum sharing, and ICT applications for international development. Dr. Takada was appointed an IEICE Fellow in 2012. He was the recipient of the Achievement Award of IEICE in 2008.

Minseok Kim (S02-M05) was born in Seoul, Korea. He received the B.S. degree in electrical engineering from Hanyang University, Seoul, Korea, and the M.E. and D.E. degrees in electrical and computer engineering from Yokohama National University (YNU), Yokohama, Japan, in 1999, 2002, and 2005, respectively. In 2007, he was an Assistant Professor with the Tokyo Institute of Technology, Tokyo, Japan, from which he was on leave at the Georgia Institute of Technology, Atlanta, GA, USA, as a Visiting Scholar in 2010. In 2014, he joined the Graduate School of Engineering, Niigata University, Niigata, Japan, as an Associate Professor. His research interests include radio propagation channel measurement and modeling, body area network, antenna array signal processing, DSP implementation on FPGAs, cognitive and software defined radios. Dr. Kim is a member of IEICE. He was the recipient of the Young Researchers Encouragement Award of IEEE VTS Japan in 2003.